Laser-Induced Cell Detachment, Patterning, and Regrowth on Gold Nanoparticle Functionalized Surfaces

Tatiana A. Kolesnikova,[†,*] Dorothee Kohler,[†] Andre G. Skirtach,[†,‡,§,*] and Helmuth Möhwald[†]

[†]Department of Interfaces, Max-Planck Institute of Colloids and Interfaces, Am Mühlenberg 1 OT Golm, D14476 Potsdam, Germany and [‡]Department of Molecular Biotechnology and [§]Center for Nano- and Biophotonics (NB-Photonics), Ghent University, Sint-Pietersnieuwstraat 33, 9000 Gent, Belgium

ABSTRACT We report on the selective cell detachment from nanoengineered gold nanoparticle (AuNP) surfaces triggered by laser irradiation, which occurs in a nonthermal manner. The gold nanoparticle-based surfaces reveal good adhesion of NIH3T3 fibroblast cells. Patterning is achieved by lithographic microcontact printing, selective gold nanoparticle deposition, and by laser beam profiling. It is shown that the effectiveness of fibroblast cell detachment depends on the cell age, laser power, and AuNP patterning profile. Heat distribution and temperature rise around gold nanoparticle functionalized surfaces is modeled, revealing low heating of nanoparticles by laser illumination. The nonthermal photochemical mechanism of cell detachment due to production of reactive oxygen species under illumination of gold nanoparticles by green laser light is studied. We also demonstrate that cells migrate from unirradiated areas leading to their reattachment and surface recovery which is important for controlled spatial organization of cells in wound healing and tissue engineering. Research presented in this work is targeted at designing biointerfaces for cell cultures.

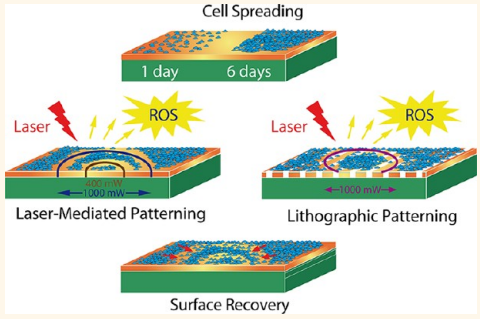

KEYWORDS: gold nanoparticles · microcontact printing · fibroblasts · laser-mediated detachment · cell patterning · cell regrowth

Targeted cell detachment is of significant interest for such areas in biomedicine as cell biology, medical implants, oncology, and tissue engineering.[1−4] Dynamic control over cell adhesion can be achieved adjusting the chemical, physical, and mechanical properties of the underlying substrate,[5] or activation of the substrate surface by different methods, such as electro-,[6−8] thermo-,[9,10] or photochemical stimuli.[11,12] For example, complete or partial detachment of human T-cells from the surface of gold and indium tin oxide (ITO) electrodes with preattached antibodies was achieved using a reductive potential.[7,8] Another way to alter cell adhesion to the substrate is light irradiation of a defined surface region which provides increased spatial control over the patterning of cells on self-assembled substrates without disturbing nonirradiated cultures of cells. This method is particularly attractive for handling/manipulation of biological samples at submillimeter scale (*i.e.*, selective cell separation, on-chip patterning, enhanced cell migration, *etc.*).[13−17] Previous studies reported application of direct UV- or near-infrared radiation for targeted cell detachment and patterning.[18−21] In the former case, cell detachment is accomplished under UV light by fabricating photoresponsive substrates from photodegradable and nontoxic polymers.[22−24] In this regard, there are some limiting factors for photodegradable polymers such as slow degradation rates; therefore, high energy is needed for their complete photodegradation. Still despite of the development of new photosensitive polymers suitable for fast and complete degradation under the UV-light, there are some disadvantages of this method, for example, irreversible alteration of the substrate surface after photodegradation and lack of biocompatibility of UV-light which can damage both the multilayer engineered structure and adherent cells.[18,19] Recently, Sada *et al.* reported on the near-IR laser triggered targeted cell detachment and collection using a carbon nanotube-based substrate,[20] where the HeLa cell detachment was initiated by photoabsorption of NIR-light by carbon nanotubes leading to photothermal conversion and photoacoustic effects. Near-IR laser irradiation

* Address correspondence to Tatiana.Kolesnikova@mpikg.mpg.de, Andre.Skirtach@mpikg.mpg.de.

Received for review June 28, 2012 and accepted October 15, 2012.

Published online October 15, 2012
10.1021/nn302891u

is biologically friendly and in combination with corresponding near-IR responsive materials appears to be an elegant and attractive method for selective laser-mediated cell harvesting and patterning in tissue engineering or on living tissues.[25−27] In other studies, the local cross-linking of biointerfaces by laser-nanoparticle interaction was reported.[28]

Another efficient method to form cell patterns is the laser induced forward transfer (LIFT) technique, where controlled transfer of material from a thin film onto a positioned nearby substrate is triggered by a highly focused pulsed laser beam.[29] A wide range of materials was used for such laser-based direct writing, including different types of living cells (such as stem cells, cancer cells, epithelial cells, *etc.*)[30−34] and biological species (*e.g.*, polymers, enzymes, proteins, DNA, *etc.*).[35−37] To induce propulsion of material, a thin layer of metal (Au, Ag, Ti, TiO_2, *etc.*) or other laser-absorbing materials, providing photothermal conversion of laser energy, is often used. Highly localized heating induces vaporization of a cell suspension and transfer of material from a support-film interface toward a receiving substrate surface. Thereby, this technique allows fabrication of cell patterns in a desired geometry; however, additional protection of cells from direct laser pulses is needed. Matrix-assisted pulsed laser evaporation direct writing (MAPLE DW) and laser-guided direct writing (LG DW) are techniques similar to LIFT, which employ pulsed UV/near-UV and IR-lasers, respectively.[38−41] Thereby, most direct cell writing techniques involve application of highly powered pulsed lasers through photothermal processes.

In this study we introduce a principally different way of tunable cell detachment and patterning *via* irradiation of AuNP functionalized surfaces by a continuous laser source, which occurs in a nonthermal manner. Application of gold nanoparticles (AuNP) is of great interest for tissue engineering;[42,43] for example, they can be used for enhancing mechanical properties or for further functionalization with organic molecules (such as fibronectin molecules) to provide enhanced cell adhesion to the substrate surface.[44,45] Gold nanoparticles possess strong photoabsorption in the green spectral range (around the surface plasmon resonance wavelength, ∼520 nm). The absorption peak shifts toward the red region for nanoparticle aggregates due to the dipole−dipole interaction on neighboring nanoparticles.[46] Thereby, AuNPs can be activated by laser irradiation with the corresponding wavelength and such a nanoplasmonic effect can lead to a strong local response in close proximity to the substrate surface (*e.g.*, photothermal conversion[47−49] or photochemical mechanism[50]), which are expected to detach cells from the substrate.

In our work fibroblast cells were chosen as a model system, which belong to a class of cells with prime duties to produce proteins for the extracellular matrix, wound healing, *etc.* For regenerative medicine and other areas, for which active control over release, detachment, and regrowth are needed, other cell types are typically explored, such as stem cells and epithelial cells. Nevertheless, fibroblasts were used in many studies, including fabrication of switchable cell culture substrates, UV-laser cell ablation from photodegradable substrates, single cell isolation by laser-induced shockwave, *etc.*[9,18,51] Here we studied the ability of NIH3T3 fibroblasts to detach selectively from AuNP-functionalized surfaces by adjusting the patterning by an incident laser beam (with 532 nm wavelength). We show that laterally controlled adhesion and detachment can be achieved by a defined distribution of light intensity, light absorbing particles, or their combination. It was found that the effectiveness of fibroblast detachment depends on the cell age, laser power density, exposure time, and AuNP patterning profile. Estimation of the temperature distribution in AuNP-based surfaces with different geometries revealed low heating of nanoparticles by laser illumination due to the low laser power density. A nonthermal photochemical mechanism of cell detachment is assigned to the production of reactive oxygen species (ROS) under illumination of Au nanoparticles by green laser light. We also demonstrate that cells can migrate from nonirradiated areas leading to their reattachment and surface recovery in time which can be important for controllable spatial organization of cells in wound healing and tissue regeneration.

RESULTS AND DISCUSSION

Nanopatterning of AuNP Surfaces. Various surfaces were used in our studies for patterning. To prepare substrates with uniform AuNP distribution, hydrophilic glass slides were covered by 8−10 nm positively charged gold nanoparticles from an aqueous colloid suspension. The optical properties of the prepared surfaces with uniformly distributed AuNPs were studied by UV−vis spectroscopy (Supporting Information, Figure S1,a). The absorption spectrum shows a single peak at 550 nm which corresponds to a slight aggregation of gold nanoparticles on the surface. The aggregation of AuNPs plays a critical role and determines their optical properties and sensing mechanism which are particularly important for biological applications of nanoparticles as sensors.[52−55] The average thickness of the uniform AuNP-based surface determined from the AFM height profile was ∼15 nm, which corresponds both to the aggregation of nanoparticles on the surface and double layer formation (Supporting Information, Figure S1,b).

The mechanism of laser−nanoparticle interaction can be mitigated and controlled by the second type of coatings used in this work. We designed stripes containing AuNPs wherein areas with and without nanoparticles were deposited alternatingly. AuNP nanoengineered

stripes were produced by microcontact printing using the polydimethylsiloxane (PDMS) stamping technique (Supporting Information, Figure S2). Such an approach allows the production of reliable and reproducible patterns of gold nanoparticles with well-defined morphology on the solid surfaces. Various molds, which can be used for PDMS stamp preparation, allow for fabrication of single- and multiline arrays of nanoparticles.

Influence of Time on Cell Adhesion. AuNP-functionalized surfaces and plain glass slides serving as controls for comparison were used for cell cultivation. To observe the cellular behavior at the early adhesion state, NIH3T3 fibroblast cells were cultured in the incubator at 37 °C under a humidified atmosphere of 5% CO_2. The morphological changes of fibroblast cell cultures were assessed during more than 3 weeks (with time intervals of ~24 h) and analyzed by a phase contrast inverted microscope. At the desired time intervals, the culture medium was drained and cells were reimmersed in a 2 mL solution of fresh DMEM medium. Cells were found to firmly adhere to both AuNP-based surfaces (with uniform distribution of AuNPs and AuNP-stripes on the surface) revealing good cell adhesion similar to a conventional control glass dish in terms of cellular spreading rate and cell morphology (Supporting Information, Figure S3).

It is obvious that the kinetics of cell spreading on the surface directly depends on the initial cell seeding density. In our studies we observed that the growth rate of the NIH3T3 fibroblasts was initially high and no significant difference was recognized for AuNP-based surfaces, where fibroblasts were attached and well spread in a similar manner. Previously, it was established that the cell adhesion process comprises three stages: the first one represents a weak adhesion stage, when fibroblast cells initially contact a substrate (this continues for around 24 h).[56,57] We found experimentally that at this stage cells are very sensitive to the ambient conditions and any significant difference in the environment can result in their detachment. The second stage is that of intermediate adhesion, that is, the phase when cells intensively spread on the surface (48−96 h). At this stage cell surface projection features (*e.g.*, lamellipodia and filopodia) can be clearly observed, indicating that the cells are highly mobile on this surface. And the final (third) phase is characterized as a strong adhesion stage, wherein cells make stress fibers and form focal adhesions (after 6−7 days of culture). For longer cell cultivation (more than 6 days of incubation), the cells for all samples reached a confluent state corresponding to microtissue formation. For quantitative analysis of cell adhesion and spreading optical images were used to calculate the number of cells in each sample. The average number of cells/cm^2 of the substrate was calculated on the basis of 10 different areas for each sample (Figure 1,a).

Cell Detachment from Uniform AuNP-Based Surfaces. Patterning of cells can be achieved by several methods, for example, by a desired distribution of nanoparticles or a specific laser beam profile. Here, we used the latter principle to show patterning by a laser beam with a ring-like profile. A round pinhole was used to form a picture with several maxima and minima of intensity arising from the diffraction of the laser beam on the aperture edges. If the size of the pinhole is small compared to the diameter of the laser beam, it will be strongly diffracted after propagating through the pinhole. For our experiments we attained a regime with two maxima of intensity; the first minimum was located in the center. Figure 1b represents a projection of the laser beam on the screen after beam expansion using a dispersing lens; the insert illustrates the intensity variation across the laser spot. This picture was obtained to confirm a ring-like profile of a laser beam using only 10% of reflected laser light (at a minimal laser power of 1 mW). Indeed, a ring-like cell detachment pattern can be observed as a result of cell irradiation on the uniform AuNP-based surface (Figure 1,c). It is still hard to compare this picture with the obtained ring-like cell detachment pattern, because any variation of pinhole diameter and position of a focal plane results in a different beam profile picture. For repeatability all the experiments were carried out under similar conditions (fixed pinhole diameter and focal plane position), so that contribution of these factors to the detachment profiles can be ignored upon discussing the other factors varied (such as power and irradiation time).

During the course of our experiments, we studied NIH3T3 fibroblast behavior under laser activation of AuNP-modified surfaces with a wavelength of 532 nm in dependence on the cell age, laser power, and irradiation time. It was found in our studies that the age of the fibroblasts drastically affects the effectiveness of their detachment by laser irradiation. Indeed, already after 6 days of incubation the cells covered the whole sample as a monolayer, whereas after 3 weeks a stable network of cells (with higher cell density on the surface) was observed due to the interconnection of their cytoskeleton leading to microtissue formation. The effect of laser irradiation (750 mW, for 2 min) was found to be much weaker for cells cultured for 3 weeks in comparison with those incubated for 6 days (Figure 1,c,d). It can be seen that the size of the ring corresponding to the laser beam profile is substantially smaller for cells grown for 3 weeks. This can be attributed to stronger intercellular links upon longer incubation time. Therefore, for all further experiments we used cells with incubation time of 6 days.

Remote activation of a uniform AuNP-based surface was conducted using a green laser (532 nm, continuous wave) with power ranging from 100 to 1000 mW and an irradiation time of 2 min. Remarkably, no visible

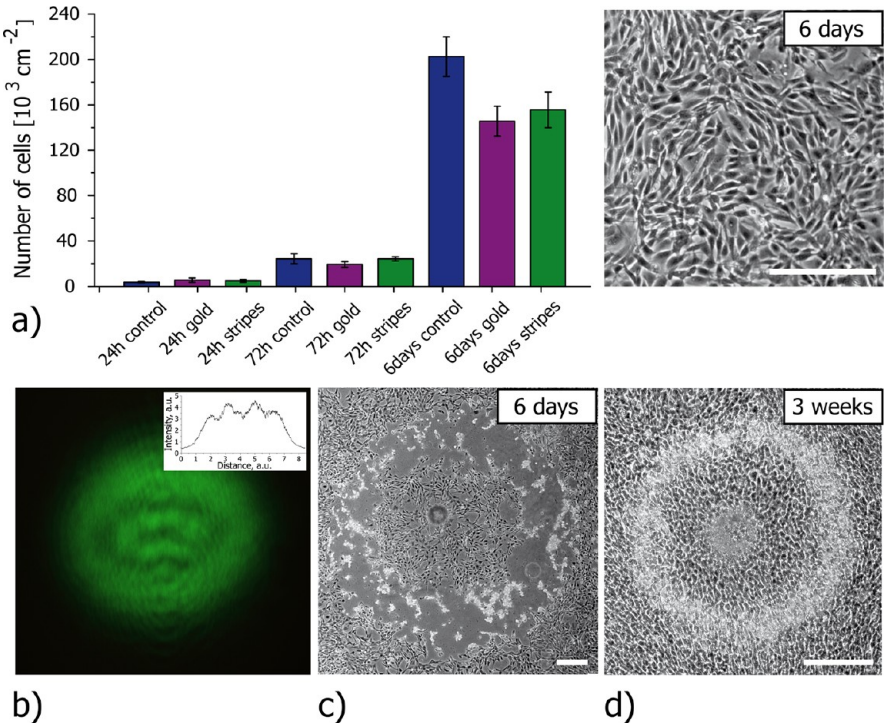

Figure 1. (a) Statistics of NIH3T3 fibroblast cell adhesion to the control glass surface, uniform AuNP-based surface, and AuNP-stripe patterned surfaces as a function of the incubation time and phase contrast microscopy image of NIH3T3 fibroblast adhesion corresponding to 6 days of cell culturing; (b) laser beam projection on the screen after beam expansion and diffraction on the round pinhole edges, revealing a few maxima (bright parts) and minima (dark parts) of intensity; the insert illustrates the intensity variation across the laser spot. Parameters on the graph are represented in arbitrary units (a.u.) to express approximate characteristic of a laser beam intensity profile; (c−d) a ring-shaped detachment of cells from the AuNP-based surfaces after laser irradiation (532 nm, 750 mW, 2 min) in dependence on the cell age (6 days and 3 weeks of culture). Pictures were obtained 24 h after surface irradiation. The scale bar for cell images is 300 μm.

effect on the cells after irradiation of the uniform AuNP-based surface was detected below 300 mW, whereas increasing laser power resulted in effective cell detachment and increasing the surface area of detachment (Figure 2). For every laser power a number of detached cells was calculated (Figure 2,a (top)). The increase of the detached area with increasing power of the laser beam (from 600 to 3100 μm for laser power varying from 400 to 1000 mW, respectively) was observed consistent with the increase of the diffraction patterns. This fact points to the existence of threshold intensity needed for cell activation/detachment and explains a broadening of area with affected cells when the intensity of the laser beam is increased. The ring-like profile of the laser beam confirms this elaboration. In addition, we observed that the time of irradiation also influences the effectiveness of fibroblast detachment (Supporting Information, Figure S4). The time of irradiation was chosen as 2 and 5 min for two different values of the incident laser beam powers (500 and 1000 mW). In both cases considerable widening of the diameter of the detached area was observed (Figure 2,a (bottom)) suggesting that detachment of cells depends not only on intensity, but also on the time of illumination (longer irradiation times influence a larger number of cells, thus increasing the surface area of detachment).

It is evident that cell detachment originates from the laser−nanoparticle interaction, because irradiation of fibroblasts on the control glass surface under the same conditions (laser power and irradiation time) did not result in their detachment (cells remained alive and unchanged on the glass slide after irradiation in the absence of AuNPs). Previous data on laser irradiation of HeLa cells with a wavelength of 514 nm revealed a similar tendency where cell death after illumination was observed only in the presence of intracellular gold nanoparticles.[50]

It was previously established that irradiation of a single-walled carbon nanotube (SWNT) coated substrate with a near-IR pulsed laser revealed a very fast detachment of HeLa cells from the substrate, where the controllability of cell detachment was associated with the SWNT ablation.[20] Also, aggregation of carbon nanotubes can lead to a significant localized temperature rise.[58] In our study AFM characterization of AuNP-based surfaces after laser irradiation revealed some physicochemical changes of surface morphology, where the first maximum of laser beam intensity was located (Supporting Information, Figure S5). Gold nanoparticles formed big aggregates (up to 100−350 nm in size) which can be assigned to movement or displacement of gold nanoparticles in the center of the

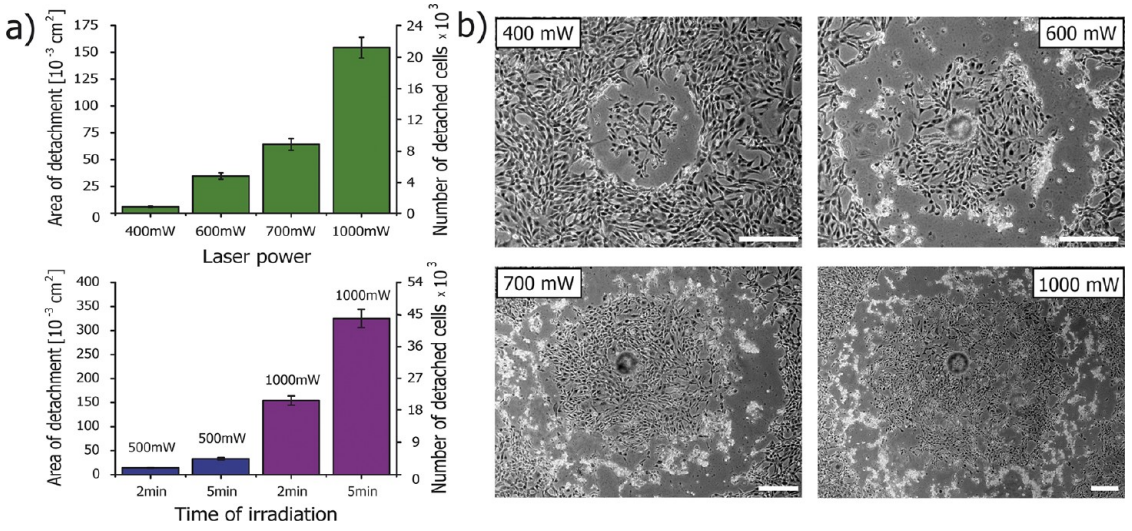

Figure 2. (a) Statistics of NIH3T3 fibroblast cell detachment from the uniform AuNP-based surface as a function of green laser power (top) and as a function of irradiation time (bottom). Average number of detached cells is calculated in dependence on the surface area of detachment and initial density of cells on the uniform AuNP-based surface before the irradiation; (b) phase contrast microscopy images of detachment areas in dependence on the laser power (400, 600, 700, and 1000 mW). The images were taken 24 h after irradiation. The scale bar for each image is 300-μm wide.

beam due to radiation pressure of light.[59] An increase of nanoparticle agglomeration (with several aggregates up to ~500 nm in size) occurred when the laser power was increased up to 1000 mW. Nevertheless, the AuNP coating remained unchanged on the surface where the second maximum of the laser beam intensity was located (even at 1000 mW) and effective detachment of cells was observed.

Cell Detachment from Stripe-Patterned AuNP-Based Surfaces. The effect of AuNP patterning on the detachment of fibroblast cells under green laser irradiation was studied using two types of stripe-patterned AuNP-based surfaces, where the ratio between the stripe width and the interstripe distance was 25:10 and 95:45 μm, respectively (Figure 3). Specifically, we show selective detachment of fibroblast cells from AuNP stripes owing to the alteration of areas covered with nanoparticles and clean glass areas in-between. Optical microscopy images show that for a sample with larger interstripe distance a small number of cells is attached to the glass surface between the AuNP-stripes, whereas complete detachment of cells from AuNP functionalized areas takes place (Figure 3,b). Therefore, varying AuNP-stripe thickness and interstripe distance represents another means of controlling patterning. For AuNP-stripe patterned surfaces a tendency similar to a substrate with uniform distribution of gold nanoparticles was observed: increasing laser power and time of irradiation resulted in increasing the detachment area and a number of detached cells, respectively. It is important to mention that for both types of AuNP stripes the effect of laser irradiation was smaller as compared to the uniform gold surface.

Theoretical Modeling of Temperature Distribution. To understand the detachment effect, we conducted theoretical modeling of the temperature rise and distribution around AuNP-functionalized surfaces with different geometries (uniform distribution of nanoparticles and AuNP stripes with different widths) (Figure 3,c). Here, the *x*-axis determines the cross section of the substrate surface along the cover glass, so that several AuNP-patterned stripes can be taken into consideration; the *z*-axis determines the distance from the AuNP patterned surface. Water was taken as the ambient medium. The temperature rise on the AuNPs was calculated on the basis of the exact analytical solution, where the temperature is directly proportional to the incident power density and absorption coefficient and inversely proportional to the distance from the nanoparticles.[53,60] Then, numerical modeling was performed to obtain the temperature distribution around the nanoparticle functionalized substrate. Our modeling reveals that stripes indeed distribute heat less efficiently than surfaces completely covered with AuNP. This effect can be clearly seen in Figure 3: temperature rise on the wider stripes is lower, while on narrower stripes it is the lowest. Thus, such stripes can be used as an additional mechanism for patterning of the surfaces. The temperature increase above the background was no more than 2 °C, revealing low heating of nanoparticles by laser illumination, which is in good agreement with previous works.[50,61]

It is well-known that the temperature rise affects cells and this effect is strain-dependent.[62,63] For mammalian fibroblasts exposed to high temperature (between 43 and 45 °C during 1 h) cell saturation density and viability were reduced significantly compared with control cells incubated at 37 °C. Furthermore, after 3 days of incubation at 47 °C no cell spreading on glass was observed.[64−66] Simanovskii *et al.* reported that the temperature at which cells can survive after 300 μs exposure by a pulsed CO_2

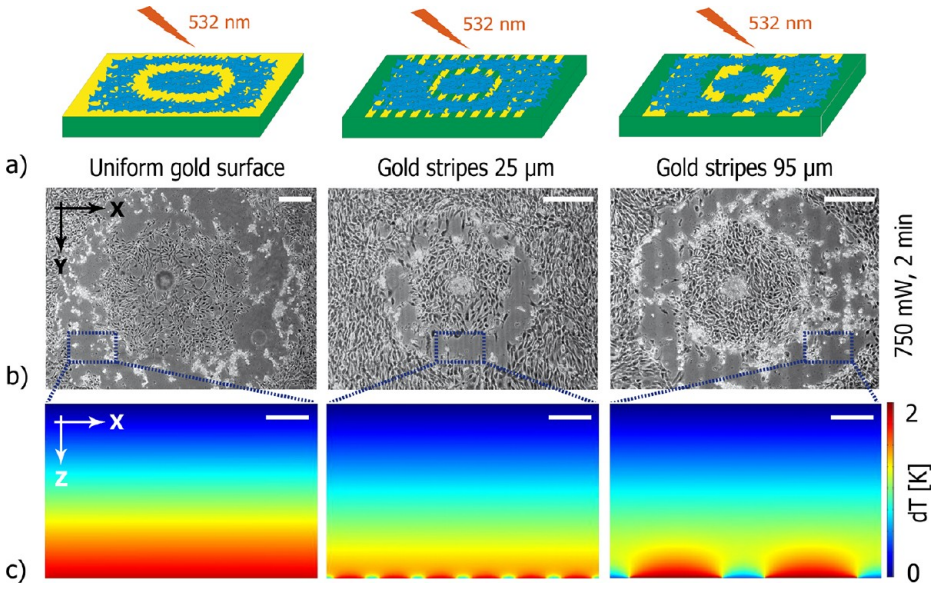

Figure 3. (a) Schematics of fibroblast cell detachment from AuNP-based surfaces (with uniform distribution of gold nanoparticles and AuNP stripes with the ratio between stripe thickness and interstripe distance of 25:10 μm and 95:45 μm, respectively); (b) phase contrast microscopy images of fibroblast detachment from the AuNP-based surfaces by green laser irradiation (750 mW, 2 min). All images were taken 24 h after laser irradiation. The scale bar for each image is 300 μm wide; (c) numerical studies of temperature distribution upon laser irradiation of AuNP-functionalized surfaces: *x*-axis determines the cross section of the substrate surface along the cover glass; *z*-axis determines the distance from the surface. Scale bar for both *x*- and *z*-axis is 50 μm width.

laser could be as high as 130 °C.[67] Principally, pulsed lasers are able to deliver far more energy in a short time frame than continuous ones. However, in our case the irradiation time was much longer (on the order of minutes) and the relevant temperature threshold terminating the cell activity (with following apoptosis) was much lower. Thus, our approach represents a simple and effective method for laser-mediated multiple cell detachment and patterning under mild conditions.

Photochemical Effect of Laser Irradiation on Cell Detachment. Laser-mediated cell detachment under low heating of AuNPs (only a few degrees) can be associated with a photochemical mechanism, such as free radicals and singlet oxygen generation, which can damage the cell membrane.[50,68−71] It was shown before that while in a vacuum under green light irradiation the photoemission of electrons from gold is hindered, the production of free radicals in electrolyte solutions can take place due to significant lowering of the energy threshold for plasmon-assisted photoemission of electrons.[72,73] This reaction occurs in the immediate vicinity to the surface of light-absorbing particles. The amount of photoelectrons and produced radicals is proportional to the volume fraction of gold nanoparticles. Because of this fact a smaller effect of laser irradiation for stripe-patterned AuNP-based surface as compared to the uniform one was observed. It is important to mention that shape, size, concentration, and aggregation of nanoparticles, along with laser power density and irradiation time can influence significantly the amount of produced reactive oxygen species (ROS), and all of these factors are interdependent.

ROS-migration is another one important moment which has to be highlighted here. We believe that there is no ROS production between the AuNP stripes and outside the laser beam area, but there is still high possibility for ROS to be mobile. They can affect neighboring cells, thereby screening the detachment effect on a stripe-patterned surface. The diffusion of generated ROS outside the critical laser intensity area can also take place. However the free radicals are very reactive, which makes them extremely unstable. The investigation the ROS formation yields, lifetimes, diffusion length, and deactivation rate constants in biological media, is very difficult due to high system heterogeneity, involving multiple deactivation processes which should be considered.[74−76] The lifetime strongly depends on the environment and it is drastically shortened in a solution compared with that in a gas phase. The ROS lifetime for biological samples can be on the order of microseconds or even nanoseconds due to very effective spin-allowed radiationless deactivation processes.[77,78] The corresponding diffusion length can be varied from tens of micrometers for the liquid phase up to nanometers inside living cells and tissues.[78] Thus, on a molecular scale ROS can be responsible for chemical reactions on a small distance from the place of their creation. Apparently, the interstripe distance in our experiments was not large enough to avoid a ROS effect on cells adhered to the glass surface in close proximity to the boundaries of AuNP stripes, thus resulting in their detachment. This is in a good agreement with Figure 3b, where complete detachment of cells took place in the case of smaller

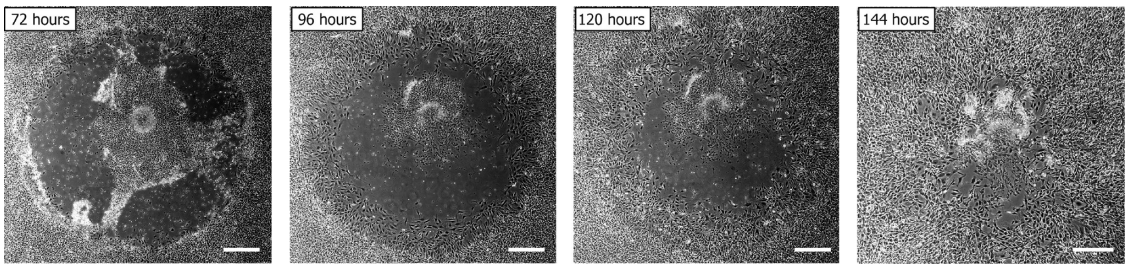

Figure 4. Surface recovery in time after laser detachment of cells (1000 mW, 2 min) from the uniform AuNP-based surface. The phase contrast microscopy images represent NIH3T3 fibroblast migration from the intact regions to the area of detachment. The images were taken every 24 h after 72, 96, 120, and 144 h, respectively. The scale bar for each image is 500-μm wide.

interstripe distance (10 μm), whereas for larger interstripe distance (25 μm) a small number of cells was still attached to the glass surface between the stripes. Albeit the diffusion length and the lifetime of ROS generated on gold stripes were small, they were still enough to affect cells between the stripes and also some neighboring cells outside the critical laser intensity area; nevertheless the area of detachment remained circular. We believe variation of stripe thickness and interstripe distance can result in a selective detachment of fibroblast cells only from AuNP stripes.

To detect ROS generation in the fibroblast cells after their exposure to the green laser light, we used redox-sensitive fluorochrome 2′,7′-dichlorofluorescein-diacetate (DCFDA) which is nonfluorescent when localized inside the cell and transforms to highly fluorescent 2′,7′-dichlorofluorescein (DCF) after oxidation (Supporting Information, Figure S6). We have shown the data for ROS production from the uniform AuNP-based surface as a control experiment which provides support for results and discussions. It is important to mention, that no ROS production was observed during the laser irradiation of cells on the control sample (without gold nanoparticles) as well as outside the illuminated AuNP-functionalized surface area.

In previous work the production of free radicals in cancer cells was detected at much lower laser power densities (55 W/cm^2) because gold nanoparticles were concentrated within the cell interior,[50] thereby plasmon-assisted photoemission of electrons inducing the ROS took place directly inside the cells. In our case light-absorbing particles were spread on the substrate surface and this reaction occurred outside the cells. Therefore at low power density the amount of ROS was not enough to affect cells, whereas at higher power densities (up to 1.5 kW/cm^2) ROS generation was responsible for their delayed apoptosis. We observed that laser irradiation (for both uniform and stripe-patterned AuNP-substrates) did not reveal immediate cell detachment. The detachment was prolonged in time and occurred gradually (Figure S7 in the Supporting Information). The following kinetics of morphological changes of the fibroblast cell culture was observed: immediately after irradiation no damaged or affected cells were found, whereas already after 1 h some cells became roundish. Over time more cells revealed conformational changes and already after 24 h all affected cells were gone from the surface, resulting in their complete detachment. This analysis indicates that such conformational changes took place due to cell signaling, which can be initiated by ROS.[79−81] There is now growing interest in ROS regulation of intracellular signaling (such as cell proliferation or differentiation, cellular survival, and oncogenic transformation).[82] Obviously, cell response to laser irradiation is difficult to study and deeper understanding insight into cell biology is required.

Surface Recovery after Laser-Induced Detachment. Subsequent surface recovery is another important aspect to be discussed here. We demonstrate that the fibroblasts can migrate from intact unirradiated regions to the "free-of-cells" areas leading to their repopulation and "surface recovery". To observe the surface recovery in time, AuNP-based surfaces with NIH3T3 fibroblasts after laser-induced patterning were stored in the incubator (37 °C, 5% CO_2) for one week and optical microscopy images were collected with 24 h intervals. Relative changes of the fibroblast cell culture after 72, 96, 120, and 144 h are represented in Figure 4. Already after 72 h cell migration from the outer intact regions into the open space created by the laser-induced cell removal was observed. Over time cells became confluent and eventually covered the entire pattern. Cell release and migration from the original pattern were shown before using Parafilm inserts, which allowed patterning of epithelial cells into desired circular and stripe patterns with following cell release from the containment pattern upon removal of the Parafilm inserts.[83] Hence laser-assisted detachment of cells represents an elegant and effective tool for controllable spatial organization of cells. It is expected to be used for a wide range of biological and engineering problems such as wound healing assays and collective cell migration.[84]

CONCLUSIONS

We have presented a simple and effective method for laser-mediated cell detachment, patterning and regrowth using nanoengineered surfaces. Substrate functionalization was performed with uniform distribution of gold nanoparticles or AuNP stripes produced by

microcontact imprinting. Multiple detachment of cells from the gold surfaces was obtained *via* green laser irradiation, depending on the cell age, laser beam power, exposure time, and AuNP-patterning profile. Cell detachment took place due to the activation of AuNPs by laser light with corresponding wavelength (nanoplasmonic effect), leading to local effects in close proximity to the substrate surface. Modeling of the temperature distribution in AuNP-based surfaces with different geometries was performed, proving low heating of NPs by laser light. A photochemical mechanism of cell membrane damaging due to production of reactive oxygen species (ROS) under illumination of AuNPs by a green laser was proved to be the reason for cell detachment. Lithographic patterning of nanoparticles was found to influence the amount of produced ROS within the periodic structures of AuNP stripes. Thereby, in this study nonthermal tunable cell detachment and patterning *via* irradiation of AuNP functionalized surfaces by a continuous laser source was introduced. Moreover, surface recovery due to migration of cells from unirradiated areas was observed, which is important for controllable spatial organization of cells, for example, in wound healing, tissue engineering, *etc.* Thereby, our study offers a new direction in investigation of cell behavior on artificially engineered gold nanoparticle-based surfaces such as laser-induced cell detachment, patterning and regrowth. We believe this technique can be applied for other cell types (such as stem cells, cancer cells, *etc.*), which are more specific and sensitive to their environment than fibroblasts, and not only for multiple cell detachment, but also for single cell operation by varying the focus area with appropriate objective lenses. We are currently exploring the possibility of producing gold nanoparticle-based surfaces responsive to the biologically friendly near-infrared wavelength region to study cell behavior under laser irradiation on the individual level.

EXPERIMENTAL SECTION

Materials. Positively charged gold nanoparticles (AuNPs) stabilized by 4-(dimethylamino) pyridine (DMAP) with a mean diameter of 8−10 nm were prepared according to previously published methods.[85] UV−vis absorption measurements showed a maximum of the surface plasmon band for AuNPs at λ_{max} = 520 nm. The concentration of the aqueous solution of AuNPs was determined to be 3×10^{13} NPs/mL. The dispersion was used without dilution. The stamp material, sylgard-184 poly(dimethylsiloxane) (PDMS) (Dow Corning GmbH, Germany) was purchased as a two-component kit, including prepolymer (base agent) and cross-linker (curing agent) components. Detergents were mixed in a 1:10 curing agent/prepolymer ratio. Stamp replication was performed in contact with a silicon masters (10×10 mm^2) (GeSiM mbH, Germany). Water was prepared in a three-stage Milipore Milli-Q Plus 185 purification system and had a resistivity higher than 18.2 MΩ·cm^{-1}.

Preparation of Gold Nanoparticle-Based Surfaces. Glass slides were initially cleaned by incubation in a piranha solution (concentrated sulfuric acid and 30% hydrogen peroxide, 1:3) at 60 °C followed by multiple rinsing with deionized water and drying in nitrogen flow. *CAUTION: Piranha solution reacts violently with organic solvents and is a skin irritant. Extreme caution should be exercised when handling the piranha solution.* After such a procedure, glass became hydrophilic by hydroxylating the surface, thus increasing the number of silanol groups on the surface. Cleaned glass slides were used as substrates for fabrication of gold nanoparticle-based surfaces. To produce substrate with uniform distribution of gold nanoparticles, gold nanoparticles were deposited on the glass slide from the aqueous colloid suspension. After 30 min of incubation substrates were thoroughly washed with deionized water and dried under nitrogen flow. Gold nanoparticle stripes on the glass surface were fabricated by microcontact printing (Supporting Information, Figure S2). PDMS stamps were prepared by mixing sylgard-184 poly(dimethylsiloxane) (PDMS) and a curing agent in a 1:10 curing agent/prepolymer ratio and degassing by applying a gentle vacuum for 30 min to remove air bubbles. Stamp replication was performed in contact with a silicon master with size 10×10 mm^2. The degassed PDMS prepolymer mixture was subsequently poured onto the silicon master and cured at 70 °C for 2 h. To obtain a hydrophilic surface after casting a PDMS replica from the silicon master, prepared PDMS stamps were oxidized by exposure to a Plasma Cleaner PDS-32 G-2 (medium 60 W) for 2 min. An aqueous dispersion of gold nanoparticles (3×10^{14} NPs/mL) was dropped onto the PDMS stamp immediately after the plasma treatment. The stamps (about 10×10 mm^2) were equilibrated for 10 min in the AuNP dispersion. The excess of gold nanoparticles was removed under a stream of filtered nitrogen. Stamping was performed manually by using tweezers for stamp handling and taking advantage of the natural stamp−substrate adhesion. The contact time was 30 min at 70 °C. Printed glass slides were post-treated at 70 °C for 10 min.

Cell Culture. Before cell culturing the substrates were sterilized by ultraviolet irradiation for 4 h in a clean bench and finally transferred to sterile culture dishes. NIH3T3 fibroblasts (by ATCC) were cultured in Dulbeco's modified eagle medium (DMEM) supplemented with 4500 mg glucose/L; 10% calf serum; 0,1% gentamicin (antibiotic). Cells were seeded in concentration of 6×10^3 cells/cm^2 and cultured in the incubator at 37 °C under a humidified atmosphere of 5% CO_2.

Experimental Techniques. Atomic force microscopy (AFM) was conducted in air at room temperature (20−25 °C) using a Nanoscope III Multimode atomic force microscope (Digital Instruments Inc., USA) operated in tapping mode. CARY 50 Conc. A UV−vis spectrometer (Varian, Germany) was used for absorption spectroscopy. Confocal laser scanning (CLSM) micrographs were taken with a Leica confocal scanning system mounted to a Leica Aristoplan (Germany) and equipped with a 63× air objective with a numerical aperture (NA) of 0.7. Control of the NIH3T3 fibroblast cell growth and spreading on the artificially engineered surfaces was conducted using a phase contrast inverted microscope Nikon Eclipse TS100 (Nikon Instruments Inc., USA) equipped with a 100× objective with NA 1.4.

Remote Laser Activation. Green-laser activation of gold nanoparticle-based surfaces was conducted using a Coherent Verdi 2W CW diode laser (Patrick Henry DR, USA) operating at 532 nm. A laser beam passing through a pinhole was settled on the sample surface through a lens (the focal distance 10 cm). Control of the NIH3T3 fibroblast cells after laser irradiation was conducted using a phase contrast inverted microscope Nikon Eclipse TS100.

Numerical Simulation of Laser-Induced Temperature Distribution. Numerical simulations of temperature distribution were performed using COMSOL multiphysics software module. The following parameters were used: heat conductivity of water, 0.5 W/m·K; laser wavelength, 532 nm; absorption coefficient of nanoparticles at 532 nm, ∼0.8 cm^{-1}; maximal incident laser power, 1000 mW; the beam radius, 0.015 cm; material parameters of gold were taken from previously reported data.[86,87] Periodic boundary conditions were used along the cover glass. Cumulative heating from neighboring nanoparticles and so-called surface-to-volume heating were taken into consideration.[88−90] It has to be noted that nanoscale heating effects can be significant when the laser beam is tightly focused to a micrometer-sized area, yielding illumination intensities on the order of 10^5−10^6 W/cm^2.[52,53,88] In this case the

effect of laser-induced cavitation can take place, resulting in a formation of gas nano- and microbubbles in close vicinity to the solid boundary.[91,92] In our study the laser beam was not focused or even deliberately defocused, thus resulting in drastically decreased laser power density. Maximal incident laser power density was estimated to be ~1.5 kW/cm^2, which is several orders of magnitude lower than those used in previous studies.

Detection of Reactive Oxygen Species (ROS). Confocal microscopy was carried out to detect ROS production in irradiated cells. Levels of intracellular ROS were analyzed using the redox-sensitive fluorochrome 2′,7′-dichlorofluorescein-diacetate (DCFDA) (Sigma). Before laser irradiation cells were incubated with 5 μM DCFDA (5 mM stock in dimethyl sulfoxide (DMSO), stored at 20 °C) in culture medium for 1 h (at 37 °C under a humidified atmosphere of 5% CO_2). After passive penetration through cell membrane, DCFDA undergoes deacetylation by intracellular esterases, resulting in a charged nonfluorescent form that is membrane impermeable and trapped inside the cells. Later it can be oxidized by ROS into highly fluorescent 2′,7′-dichlorofluorescin (DCF). After loading with DCFDA, cells were gently washed by phosphate buffered saline (PBS) (pH 7.4) and placed in fresh complete DMEM media. After performing laser irradiation, cells were returned to the incubator (for up to 24 h). The fluorescence was then measured at an excitation wavelength 488 nm and an emission wavelength 535 nm using a confocal laser scanning microscope (Leica Aristoplan, Germany).

Conflict of Interest: The authors declare no competing financial interest.

Acknowledgment. The authors thank Anneliese Heilig for AFM measurements and Christine Pilz-Allen (MPIKG, Golm) for cell culture preparation and maintenance.

Supporting Information Available: Additional figures as described in the text. This material is available free of charge *via* the Internet at http://pubs.acs.org.

REFERENCES AND NOTES

1. *Tissue Engineering: From Lab to Clinic*; Pallua, N., Suschek, C. V., Eds.; Springer: New York, USA, 2011.
2. *Introduction to Cell and Tissue Culture: Theory and Technique*; Mather, J. P., Roberts, P. E., Eds.; Springer: New York, USA, 1998.
3. Liu, W. F.; Chen, C. S. Engineering Biomaterials to Control Cell Function. *Mater. Today* **2005**, *8*, 28–35.
4. Tang, Z. Y.; Wang, Y.; Podsiadlo, P.; Kotov, N. A. Biomedical Applications of Layer-by-Layer Assembly: From Biomimetics to Tissue Engineering. *Adv. Mater.* **2006**, *18*, 3203–3224.
5. Gribova, V.; Auzely-Velty, R.; Picart, C. Polyelectrolyte Multilayer Assemblies on Materials Surfaces: From Cell Adhesion to Tissue Engineering. *Chem. Mater.* **2012**, *24* (5), 854–869.
6. Wildt, B.; Wirtz, D.; Searson, P. C. Triggering Cell Detachment from Patterned Electrode Arrays by Programmed Subcellular Release. *Nat. Protoc.* **2010**, *5*, 1273–1280.
7. Zhu, H.; Yan, J.; Revzin, A. Catch and Release Cell Sorting: Electrochemical Desorption of T-Cells from Antibody-Modified Microelectrodes. *Coll. Surf. B* **2008**, *64*, 260–268.
8. Shah, S. S.; Lee, J. Y.; Verkhoturov, S.; Tuleuova, N.; Schweikert, E. A.; Ramanculov, E.; Revzin, A. Exercising Spatiotemporal Control of Cell Attachment with Optically Transparent Microelectrode. *Langmuir* **2008**, *24*, 6837–6844.
9. Schmidt, S.; Zeiser, M.; Hellweg, T.; Duschl, C.; Fery, A.; Möhwald, H. Adhesion and Mechanical Properties of PNIPAM Microgel Films and their Potential Use as Switchable Cell Culture Substrates. *Adv. Funct. Mater.* **2010**, *20*, 3235–3243.
10. Yamato, M.; Konno, C.; Utsumi, M.; Kikuchi, A.; Okano, T. Thermally Responsive Polymer-Grafted Surfaces Facilitate Patterned Cell Seeding and Co-culture. *Biomaterials* **2002**, *23*, 561–567.
11. Mendelsohn, J. D.; Yang, S. Y.; Hiller, J.; Hochbaum, A. I.; Rubner, M. F. Rational Design of Cytophilic and Cytophobic Polyelectrolyte Multilayer Thin Films. *Biomacromolecules* **2003**, *4*, 96–106.
12. Robertus, J.; Browne, W. R.; Feringa, B. L. Dynamic Control Over Cell Adhesive Properties Using Molecular-Based Surface Engineering Strategies. *Chem. Soc. Rev.* **2010**, *39*, 354–378.
13. Berns, M. W.; Wright, W. H.; Wiegand-Steubing, R. Laser Microbeam as a Tool in Cell Biology. *Int. Rev. Cytol.* **1992**, *129*, 1–44.
14. Horneffer, V.; Linz, N.; Vogel, A. Principles of Laser-Induced Separation and Transport of Living Cells. *J. Biomed. Optics* **2007**, *12*, 054016.
15. El-Ali, J.; Sorger, P. K.; Jensen, K. F. Cells on Chips. *Nature* **2006**, *442*, 403–411.
16. Ho, C. T.; Lin, R. Z.; Chang, W. Y.; Chang, H. Y.; Liu, C. H. Rapid Heterogeneous Liver-Cell on-Chip Patterning *via* the Enhanced Field-Induced Dielectrophoresis Trap. *Lab Chip* **2006**, *6*, 724–734.
17. Lauffenburger, D. A.; Horwitz, A. F. Cell Migration: A Physically Integrated Molecular Process. *Cell* **1996**, *84*, 359–369.
18. Pasparakis, G.; Manouras, T.; Selimis, A.; Vamvakaki, M.; Argitis, P. Laser-Induced Cell Detachment and Patterning with Photodegradable Polymer Substrates. *Angew. Chem., Int. Ed.* **2011**, *50*, 4142–4145.
19. Nakanishi, J.; Kikuchi, Y.; Takarada, T.; Nakayama, H.; Yamaguchi, K.; Maeda, M. Spatiotemporal Control of Cell Adhesion on a Self-Assembled Monolayer Having a Photocleavable Protecting Group. *Anal. Chim. Acta* **2006**, *578*, 100–104.
20. Sada, T.; Fujigaya, T.; Niidome, Y.; Nakazawa, K.; Nakashima, N. Near-IR Laser-Triggered Target Cell Collection Using a Carbon Nanotube-Based Cell-Cultured Substrate. *ACS Nano* **2001**, *5*, 4414–4421.
21. Gu, L.; Ingle, N.; Mohantya, S. K. Detachment and Reorientation of Cells Using Near-Infrared Laser Microbeam. *J. Biomed. Optics* **2001**, *16*, 115002.
22. Wirkner, M.; Alonso, J. M.; Maus, V.; Salierno, M.; Lee, T. T.; García, A. J.; del Campo, A. Triggered Cell Release from Materials Using Bioadhesive Photocleavable Linkers. *Adv. Mater.* **2011**, *23*, 3907–3910.
23. Kloxin, A. M.; Kasko, A. M.; Salinas, C. N.; Anseth, K. S. Photodegradable Hydrogels for Dynamic Tuning of Physical and Chemical Properties. *Science* **2009**, *324*, 59–63.
24. Ercole, F.; Evans, R. A.; Davis, T. P. Photoresponsive Materials: Photochromic Polymers, Light-Triggered Self-Assembly, Surface Modification, Fluorescence Modulation and Beyond. *Polym. Chem.* **2010**, *1*, 37–54.
25. Moon, H. K.; Lee, S. H.; Choi, H. C. *In Vivo* Near-Infrared Mediated Tumor Destruction by Photothermal Effect of Carbon Nanotubes. *ACS Nano* **2009**, *3*, 3707–3713.
26. Thalhammer, S.; Lahr, G.; Clement-Sengewald, A.; Heckl, W. M.; Burgemeister, R.; Schutze, K. Laser Microtools in Cell Biology and Molecular Medicine. *Laser Phys.* **2003**, *13*, 681–691.
27. Vogel, A.; Lorenz, K.; Horneffer, V.; Huttmann, G.; von Smolinski, D.; Gebert, A. Mechanisms of Laser-Induced Dissection and Transport of Histologic Specimens. *Biophys. J.* **2007**, *93*, 4481–4500.
28. Skirtach, A. G.; Volodkin, D. V.; Möhwald, H. Bio-Interfaces-Interaction of PLL/HA Thick Films with Nanoparticles and Microcapsules. *Chem. Phys. Chem.* **2010**, *11*, 822–829.
29. Schiele, N. R.; Corr, D. T.; Huang, Y.; Raof, N. A.; Xie, Y.; Chrisey, D. B. Laser-Based Direct-Write Techniques for Cell Printing. *Biofabrication* **2010**, *2*, 032001 (14 pp).
30. Ringeisen, B. R.; Kim, H.; Barron, J. A.; Krizman, D. B.; Chrisey, D. B.; Jackman, S.; Auyeung, R. Y. C.; Spargo, B. J. Laser Printing of Pluripotent Embryonal Carcinoma Cells. *Tissue Eng.* **2004**, *10*, 483–491.
31. Hopp, B.; Smausz, T.; Kresz, N.; Barna, N.; Bor, Z.; Kolozsvári, L.; Chrisey, D. B.; Szabó, A.; Nógrádi, A. Survival and Proliferative Ability of Various Living Cell Types after Laser-Induced Forward Transfer. *Tissue Eng.* **2005**, *11*, 1817–1823.
32. Ringeisen, B. R.; Othon, C. M.; Barron, J. A.; Young, D.; Spargo, B. J. Jet-Based Methods to Print Living Cells. *Biotechnol. J.* **2006**, *1*, 930–948.

33. Ovsianikov, A.; Gruene, M.; Pflaum, M.; Koch, L.; Maiorana, F.; Wilhelmi, M.; Haverich, A.; Chichkov, B. Laser Printing of Cells into 3D Scaffolds. *Biofabrication* **2010**, *2*, 014104.
34. Koch, L.; Kuhn, S.; Sorg, H.; Gruene, M.; Schlie, S.; Gaebel, R.; Polchow, B.; Reimers, K.; Stoelting, S.; Ma, N.; *et al*. Laser Printing of Skin Cells and Human Stem Cells. *Tissue Eng. C Methods* **2010**, *16*, 847–854.
35. Fernandez-Pradas, J. M.; Colina, M.; Serra, P.; Dominguez, J.; Morenza, J. L. Laser-Induced Forward Transfer of Biomolecules. *Thin Solid Films* **2004**, *453*−*454*, 27–30.
36. Barron, J. A.; Young, H. D.; Ringeisen, B. R.; Dlott, D. D.; Krizman, D. B. Biological Laser Printing as an Alternative to Traditional Protein Arrayers. *Proc. SPIE* **2005**, *5699*, 517–525.
37. Duocastella, M.; Colina, M.; Fernandez-Pradas, J. M.; Serra, P.; Morenza, J. L. Study of the Laser-Induced Forward Transfer of Liquids for Laser Bioprinting. *Appl. Surf. Sci.* **2007**, *253*, 7855–7859.
38. Barron, J. A.; Ringeisen, B. R.; Kim, H. S.; Spargo, B. J.; Chrisey, D. B. Application of Laser Printing to Mammalian Cells. *Thin Solid Films* **2004**, *453*−*454*, 383–387.
39. Chrisey, D. B.; Piqué, A.; McGill, R. A.; Horwitz, J. S.; Ringeisen, B. R.; Bubb, D. M.; Wu, P. K. Laser Deposition of Polymer and Biomaterial Films. *Chem. Rev.* **2003**, *103*, 553–576.
40. Nahmias, Y.; Odde, D. J. Micropatterning of Living Cells by Laser-Guided Direct Writing: Application to Fabrication of Hepatic Endothelial Sinusoid-like Structures. *Nat. Protoc.* **2006**, *1*, 2288–2296.
41. Nahmias, Y.; Schwartz, R. E.; Verfaillie, C. M.; Odde, D. J. Laser-Guided Direct Writing for Three-Dimensional Tissue Engineering. *Biotechnol. Bioeng.* **2005**, *92*, 129–136.
42. Murphy, C. J.; Gole, A. M.; Stone, J. W.; Sisco, P. N.; Alkilany, A. M.; Goldsmith, E. C.; Baxter, S. C. Gold Nanoparticles in Biology: Beyond Toxicity to Cellular Imaging. *Acc. Chem. Res.* **2008**, *41*, 1721–1730.
43. Guo, S.; Wang, E. Functional Micro/Nanostructures: Simple Synthesis and Application in Sensors, Fuel Cells, and Gene Delivery. *Acc. Chem. Res.* **2011**, *44*, 491–500.
44. Lee, H.; Jang, Y.; Seo, J.; Nam, J.-M.; Char, K. Nanoparticle-Functionalized Polymer Platform for Controlling Metastatic Cancer Cell Adhesion, Shape, and Motility. *ACS Nano* **2011**, *5*, 5444–5456.
45. Wittmer, C. R.; Phelps, J. A.; Saltzman, W. M.; Van Tassel, P. R. Fibronectin Terminated Multilayer Films: Protein Adsorption and Cell Attachment Studies. *Biomaterials* **2007**, *28*, 851–860.
46. Quinten, M.; Kreibig, U. Optical Properties of Aggregates of Small Metal Particles. *Surf. Sci.* **1986**, *172*, 557–577.
47. Urban, A. S.; Fedoruk, M.; Horton, M. R.; Radler, J.; Stefani, F. D.; Feldmann, J. Controlled Nanometric Phase Transitions of Phospholipid Membranes by Plasmonic Heating of Single Gold Nanoparticles. *Nano Lett.* **2009**, *9*, 2903–2908.
48. Volodkin, D. V.; Delcea, M.; Möhwald, H.; Skirtach, A. G. Remote Activation of Hyaluronic Acid/Poly-L-lysine Films and Microcapsules. *ACS Mater. Int. Sci.* **2009**, *1*, 1705–1710.
49. Alessandri, I.; Depero, L. E. Laser-Induced Modification of Polymeric Beads Coated with Gold Nanoparticles. *Nanotechnology* **2008**, *19*, 305301.
50. Krpetić, Ž; Nativo, P.; Sée, V.; Prior, I. A.; Brust, M.; Volk, M. Inflicting Controlled Nonthermal Damage to Subcellular Structures by Laser-Activated Gold Nanoparticles. *Nano Lett.* **2010**, *10*, 4549–4554.
51. Hosokawa, Y.; Takabayashi, H.; Miura, S.; Shukunami, C.; Hiraki, Y.; Masuhara, H. Nondestructive Isolation of Single Cultured Animal Cells by Femtosecond Laser-Induced Shockwave. *Appl. Phys. A: Mater. Sci. Process.* **2004**, *79*, 795–798.
52. Delcea, M.; Sternberg, N.; Yashchenok, A. M.; Georgieva, R.; Bäumler, H.; Möhwald, H.; Skirtach, A. G. Nanoplasmonics for Dual-Molecule Release through Nanopores in the Membrane of Red Blood Cells. *ACS Nano* **2012**, *6*, 4169–4180.
53. Skirtach, A. G.; Dejugnat, C.; Braun, D.; Susha, A. S.; Rogach, A. L.; Parak, W. J.; Möhwald, H.; Sukhorukov, G. B. The Role of Metal Nanoparticles in Remote Release of Encapsulated Materials. *Nano Lett.* **2005**, *5*, 1371–1377.
54. Rivera Gil, P.; del Mercato, L. L.; del-Pino, P.; Munoz-Javier, A.; Parak, W. J. Nanoparticle-Modified Polyelectrolyte Capsules. *Nano Today* **2008**, *3*, 12–21.
55. Preiss, M. R.; Bothun, G. D. Stimuli-Responsive Liposome-Nanoparticle Assemblies. *Expert Opin. Drug Delivery* **2011**, *8*, 1025–1040.
56. Murphy-Ullrich, J. E. The De-adhesive Activity of Matricellular Proteins: Is Intermediate Cell Adhesion an Adaptive State? *J. Clin. Invest.* **2011**, *107*, 785–790.
57. *Cell Adhesion, Frontiers in Molecular Biology*; Beckerle, M. C., Ed.; Oxford University Press: New York, USA, 2001.
58. Sun, Y.; Skirtach, A. G.; Seki, T.; Yagai, S.; Li, H. G.; Möhwald, H.; Nakanishi, T. Fullerenes/Carbon Nanotube Assemblies as Photothermal Conversion Sensors. *J. Am. Chem. Soc.* **2010**, *132*, 8566–8569.
59. Lebedev, P. N. Experimental Examination of Light Pressure. *Ann. Phys.* **1901**, *6*, 26.
60. Goldenberg, H.; Tranter, C. J. Heat Flow in an Infinite Medium Heated by a Sphere. *British J. Appl. Phys.* **1952**, *3*, 296–298.
61. Keblinski, P.; Cahill, D. G.; Bodapati, A.; Sullivan, C. R.; Taton, T. A. Limits of Localized Heating by Electromagnetically Excited Nanoparticles. *J. Appl. Phys.* **2006**, *100*, 054305.
62. Stephenson, N. G. Effects of Temperature on Reptilian and Other Cells. *J. Embryol. Exp. Morphol.* **1966**, *16*, 455–467.
63. Thompson, K. V. A.; Holliday, R. Effect of Temperature on the Longevity of Human Fibroblasts in Culture. *Exp. Cell Res.* **1973**, *80*, 354–360.
64. Hara, H.; Lamon, K. D.; Kaji, H. Effect of Temperature on Normal and SV40-Transformed Human Fibroblasts. *Biochim. Biophys. Acta* **1981**, *673*, 37–45.
65. Yamasaki, H.; Got, M.; Yoshihara, T.; Sekiguchi, M.; Konno, K.; Momoi, Y.; Iwasaki, T. Exercise-Induced Superficial Digital Flexor Tendon Hyperthermia and the Effect of Cooling Sheets on Thoroughbreds. *J. Equine Sci.* **2001**, *12*, 85–91.
66. Zhang, L.; Zhou, X.; Wang, Q.; Wang, Y.; Tang, L.; Huang, D. Effect of Heat Stress on the Expression Levels of Receptor Activator of NF-jB Ligand and Osteoprotegerin in Human Periodontal Ligament Cells. *Int. Endodontic J.* **2012**, *45*, 68–75.
67. Simanovskii, D. M.; Mackanos, M. A.; Irani, A. R.; O'Connell-Rodwell, C. E.; Contag, C. H.; Schwettman, H. A.; Palanker, D. V. Cellular Tolerance to Pulsed Hyperthermia. *Phys. Rev. E* **2006**, *74*, 011915.
68. Dolmans, D.; Fukumura, D.; Jain, R. K. Photodynamic Therapy for Cancer. *Nature Rev.* **2003**, *3*, 380–387.
69. Berg, K.; Folini, M.; Prasmickaite, L.; Selbo, P. K.; Bonsted, A.; Engesaeter, B. O.; Zaffaroni, N.; Weyergang, A.; Dietze, A.; Maelandsmo, G. M.; *et al*. Photochemical Internalization: A New Tool for Drug Delivery. *Curr. Pharm. Biotechnol.* **2007**, *8*, 362–372.
70. Febvay, S.; Marini, D. M.; Belcher, A. M.; Clapham, D. E. Targeted Cytosolic Delivery of Cell-Impermeable Compounds by Nanoparticle-Mediated, Light-Triggered Endosome Disruption. *Nano Lett.* **2010**, *10*, 2211–2219.
71. Misawa, M.; Takahashi, J. Generation of Reactive Oxygen Species Induced by Gold Nanoparticles under X-ray and UV Irradiations. *Nanomed: Nanotechnol. Biol. Med.* **2011**, *7*, 604–614.
72. Brodsky, A. M.; Pleskov, Y. V. In *Progress in Surface Science*; Davison, S. G., Ed.; Pergamon Press: Oxford, UK, 1972; Vol. 2.
73. Henglein, A. Physicochemical Properties of Small Metal Particles in Solution: "Microelectrode" Reactions, Chemisorption, Composite Metal Particles, and the Atom-to-Metal Transition. *J. Phys. Chem.* **1993**, *97*, 5457–5471.
74. Wardman, P. Fluorescent and Luminescent Probes for Measurement of Oxidative and Nitrosative Species in Cells and Tissues: Progress, Pitfalls, and Prospects. *Free Radical Biol. Med.* **2007**, *43*, 995–1022.
75. Blokhina, O.; Virolainen, E.; Fagerstedt, K. V. Antioxidants, Oxidative Damage and Oxygen Deprivation Stress: A Review. *Ann. Bot.* **2003**, *91*, 179–194.

76. Zurgil, N.; Shafran, Y.; Afrimzon, E.; Fixler, D.; Shainberg, A.; Deutsch, M. Concomitant Real-Time Monitoring of Intracellular Reactive Oxygen Species and Mitochondrial Membrane Potential in Individual Living Promonocytic Cells. *J. Immunol. Met.* **2006**, *316*, 27–41.
77. Wilkinson, F.; Helman, P. W.; Ross, A. B. Rate Constants for the Decay and Reactions of the Lowest Electronically Excited Singlet State of Molecular Oxygen in Solution. An Expanded and Revised Computation. *J. Phys. Chem. Ref. Data* **1995**, *24*, 663–677.
78. Schweitzer, C.; Schmidt, R. Physical Mechanisms of Generation and Deactivation of Singlet Oxygen. *Chem. Rev.* **2003**, *103*, 1685–1757.
79. DeMali, K.; Wennerberg, K.; Burridge, K. Integrin Signaling to the Actin Cytoskeleton. *Curr. Opin. Cell Biol.* **2003**, *15*, 572–582.
80. Brown, A. E. X.; Discher, D. E. Conformational Changes and Signaling in Cell and Matrix Physics. *Curr. Biol.* **2009**, *19*, R781–R789.
81. Torres, A. J.; Wu, M.; Holowka, D.; Baird, B. Nanobiotechnology and Cell Biology: Micro- and Nanofabricated Surfaces to Investigate Receptor-Mediated Signaling. *Annu. Rev. Biophys.* **2008**, *37*, 265–288.
82. Hamanaka, R. B.; Chandel, N. S. Mitochondrial Reactive Oxygen Species Regulate Cellular Signaling and Dictate Biological Outcomes. *Trends Biochem. Sci.* **2010**, *35*, 505–513.
83. Javaherian, S.; O'Donnell, K. A.; McGuigan, A. P. A Fast and Accessible Methodology for Micro-patterning Cells on Standard Culture Substrates Using Parafilm Inserts. *PLoS* **2011**, *6*, 1–8.
84. Poujade, M.; Grasland-Mongrain, E.; Hertzog, A.; Jouanneau, J.; Chavrier, P.; Ladoux, B.; Buguin, A.; Silberzan, P. Collective Migration of an Epithelial Monolayer in Response to a Model Wound. *Proc. Natl. Acad. Sci. U.S.A.* **2007**, *104*, 15988–15993.
85. Gittins, D.; Caruso, F. Spontaneous Phase Transfer of Nanoparticulate Metals from Organic to Aqueous Media. *Angew. Chem., Int. Ed.* **2001**, *40*, 3001–3004.
86. Johnson, P. B.; Christy, R. W. Optical Constants of the Noble Metals. *Phys. Rev. B* **1972**, *6*, 4370–4379.
87. Baffou, G.; Rigneault, H. Femtosecond-Pulsed Optical Heating of Gold Nanoparticles. *Phys. Rev. B* **2011**, *84*, 035415.
88. Govorov, A. O.; Zhang, W.; Skeini, T.; Richardson, H.; Lee, J.; Kotov, N. Gold Nanoparticle Ensembles as Heaters and Actuators: Melting and Collective Plasmon Resonances. *Nanoscale Res. Lett.* **2006**, *1*, 84–90.
89. Govorov, A. O.; Richardson, H. H. Generating Heat with Metal Nanoparticles. *Nano Today* **2007**, *2*, 30–38.
90. Bedard, M. F.; Braun, D.; Sukhorukov, G. B.; Skirtach, A. G. Towards Self-Assembly of Nanoparticles on Polymeric Capsules: Release Threshold and Permeability. *ACS Nano* **2008**, *2*, 1807–1816.
91. Vogel, A.; Lauterborn, W. Acoustic Transient Generation by Laser-Produced Cavitation Bubbles Near Solid Boundaries. *J. Acoust. Soc. Am.* **1988**, *84*, 719–731.
92. Vogel, A.; Lauterborn, W.; Timm, R. Optical and Acoustic Investigations of the Dynamics of Laser-Produced Cavitation Bubbles near a Solid Boundary. *J. Fluid Mech.* **1989**, *206*, 299–338.